1-1-2016

Experimental and discrete element modelling of geocell-stabilized subballast subjected to cyclic loading

Ngoc Trung Ngo
University of Wollongong, trung@uow.edu.au

Buddhima Indraratna
University of Wollongong, indra@uow.edu.au

Cholachat Rujikiatkamjorn
University of Wollongong, cholacha@uow.edu.au

M. Mahdi Biabani
University of Wollongong, mmb958@uowmail.edu.au

Experimental and discrete element modelling of geocell-stabilized subballast subjected to cyclic loading

Abstract

This paper presents a study of the load-deformation behaviour of geocell-stabilised sub-ballast subjected to cyclic loading using a novel track process simulation apparatus. The tests were conducted at frequencies varying from 10-30 Hz. This frequency range is generally representative of Australian Standard Gauge trains operating up to 160 km/h. The discrete element method (DEM) was also used to model geocell-reinforced sub-ballast under plane strain conditions. The geocell was modelled by connecting a group of small circular balls together to form the desired geometry and aperture using contact and parallel bonds. Tensile and bending tests were carried out to calibrate the model parameters adopted for simulating geocell. To model irregularly-shaped particles of sub-ballast, clusters of bonded circular balls were used. The simulated load-deformation curves of the geocell-reinforced sub-ballast assembly at varying cyclic load cycles were in good agreement with the experimental observations. The results indicated that geocell decreased the vertical and lateral deformation of sub-ballast assemblies at any given frequency. Furthermore, the DEM can also provide an insight into the distribution of contact force chains, and average contact normal and shear force distributions, which cannot be determined experimentally.

Disciplines

Engineering | Science and Technology Studies

Publication Details

Ngo, N., Indraratna, B., Rujikiatkamjorn, C. & Biabani, M. Mahdi. (2016). Experimental and discrete element modelling of geocell-stabilized subballast subjected to cyclic loading. Journal of Geotechnical and Geoenvironmental Engineering, 142 (4), 04015100-1-04015100-14.

Experimental and discrete element modelling of geocell-stabilised sub-ballast under cyclic loading

Ngoc Trung Ngo, PhD, MEng, BEng

Lecturer, Centre for Geomechanics and Railway Engineering, Faculty of Engineering, University of Wollongong, Wollongong City, NSW 2522, Australia; ARC Centre for Excellence for Geotechnical Science and Engineering, Australia Faculty of Engineering, Australia

Buddhima Indraratna, PhD (Alberta), FIEAust.,FTSE, FASCE

Research Director, Professor of Civil Engineering, Centre for Geomechanics and Railway Engineering, Faculty of Engineering, University of Wollongong, Wollongong, NSW 2522, Australia. ARC Centre for Excellence for Geotechnical Science and Engineering, Australia

Cholachat Rujikiatkamjorn, PhD, MEng, BEng

Associate Professor, Centre for Geomechanics and Railway Engineering, Faculty of Engineering, University of Wollongong, Wollongong City, NSW 2522, Australia; ARC Centre for Excellence for Geotechnical Science and Engineering, Australia Faculty of Engineering, Australia

Mohammad Mahdi Biabani, PhD candidate, MEng, BEng
PhD student, Centre for Geomechanics and Railway Engineering, Faculty of Engineering, University of Wollongong, Wollongong City, NSW 2522, Australia; ARC Centre for Excellence for Geotechnical Science and Engineering, Australia Faculty of Engineering, Australia

Technical paper Submitted to: Journal of Geotechnical and Geoenvironmental Engineering ASCE

Author for correspondence:
Prof. B. Indraratna
Faculty of Engineering
University of Wollongong
Wollongong, NSW 2522
Australia.
Ph: +61 2 4221 3046
Fax: +61 2 4221 3238
Email: indra@uow.edu.au

Experimental and discrete element modelling of geocell-stabilised sub-ballast under cyclic loading

Ngoc Trung Ngo[1], Buddhima Indraratna[2], Cholachat Rujikiatkamjorn[3], and M. Mahdi Biabani[4]

[1]Lecturer, Centre for Geomechanics and Railway Engineering, Faculty of Engineering and Information Sciences, ARC Centre of Excellence for Geotechnical Science and Engineering University of Wollongong, Wollongong, NSW 2522, Australia. Email: trung@uow.edu.au, Ph: +61 2 4221 4892 Fax: +61 2 4221 3238

[2]Research Director, Professor of Civil Engineering, Centre for Geomechanics and Railway Engineering, Faculty of Engineering, University of Wollongong, Wollongong, NSW 2522, Australia. ARC Centre for Excellence for Geotechnical Science and Engineering, Australia, Email: indra@uow.edu.au, Ph: +61 2 4221 3046 Fax: +61 2 4221 3238

[3]Associate Professor, Centre for Geomechanics and Railway Engineering, Faculty of Engineering and Information Sciences, ARC Centre of Excellence for Geotechnical Science and Engineering, University of Wollongong, Wollongong, NSW 2522, Australia. Email: cholacha@uow.edu.au, Ph: +61 2 4221 5852 Fax: +61 2 4221 3238

[4]PhD Candidate, Centre for Geomechanics and Railway Engineering, Faculty of Engineering, University of Wollongong, Wollongong City, NSW 2522, Australia; ARC Centre for Excellence for Geotechnical Science and Engineering, Australia Faculty of Engineering, Australia .Email: mmb958@uowmail.edu.au

ABSTRACT

This paper presents a study of the load-deformation behaviour of geocell-stabilised sub-ballast subjected to cyclic loading using a novel track process simulation apparatus. The tests were conducted at frequencies varying from 10–30 Hz. This frequency range is generally representative of Australian Standard Gauge trains operating up to 160 km/h. The discrete element method (DEM) was also used to model geocell-reinforced sub-ballast under plane strain conditions. The geocell was modelled by connecting a group of small circular balls together to form the desired geometry and aperture using contact and parallel bonds. Tensile and bending tests were carried out to calibrate the model parameters adopted for simulating geocell. To model irregularly-shaped particles of sub-ballast, clusters of bonded circular balls were used. The simulated load-deformation curves of the geocell-reinforced sub-ballast assembly at varying cyclic load cycles were in good agreement with

the experimental observations. The results indicated that geocell decreased the vertical and lateral deformation of sub-ballast assemblies at any given frequency. Furthermore, the DEM can also provide an insight into the distribution of contact force chains, and average contact normal and shear force distributions, which cannot be determined experimentally.

Introduction

A railway track network plays an important role in the transportation infrastructure worldwide. A ballasted railway track is commonly used for several reasons, including economical construction cost, and ease of maintenance. The layer of sub-ballast underneath the ballast helps to transmit and distribute the wheel load from the sleepers to the underlaying subgrade (Selig and Waters 1994; Indraratna *et al.* 2013; Suiker *et al*. 2005). The sub-ballast normally consists of broadly graded, naturally occurring or processed mixtures of sand and gravel, or slag, that is intended to act as a stress reduction layer (capping layer) and to prevent mutual penetration or intermixing of the subgrade (Trani and Indraratna 2010; Indraratna *et al.* 2011a). Moreover, the sub-ballast must also be permeable enough to avoid a build up of excess pore pressure under repeated loads, and an accumulation in the moisture content. Upon repeated train loading, sub-ballast aggregates become degraded and fouled by the progressive accumulation of external fine particles or mud-pumping of soft subgrade, which seriously decreases the shear strength and drainage capacity of the track (Indraratna *et al*. 2011b). This action would change the gradation of sub-ballast, reduce its porosity, and further inhibit drainage. Among several problems, tracks are constantly subjected to the spreading out of ballast and sub-ballast aggregates due to vibration from repeated wheel loads, coupled with lateral and longitudinal forces exerted on the track. This results in excessive differential settlement which eventually alters the

geometry of the track and leads to track instability (Lackenby *et al*. 2007; Anderson and Fair 2008). To mitigate this issue, the sub-ballast must be designed to prevent any intermixing of ballast and subgrade using a proper sub-ballast gradation and thickness (Selig and Waters 1994; Indraratna *et al.* 2011a).

In recent decades high strength geosynthetic reinforcement has been widely used in the substructural layers to strengthen the substructure of rail tracks (Bathurst and Raymond 1987; Ashmawy and Bourdeau 1995; Giroud and Han 2004; Koerner 2005; Fernandes *et al.* 2008; Pokharel *et al.* 2010; Ngo *et al.* 2014; ; Indraratna *et al*. 2015). Indeed, it was reported that geosynthetics could provide additional confinement onto the ballast/sub-ballast layers and thus reduce the vertical and lateral deformation of the track (Indraratna *et al.* 2011a). Geocell, a type of geosynthetics manufactured in the form of three-dimensional interconnected honeycomb polymeric cells, could be used as a reinforcement to further improve the load-bearing capacity and also reduce the overall deformation of tracks over weak soil deposits. Owing to its three-dimensional configuration, geocell arrests lateral spreading of the in-fill materials and creates a relatively stiffer mat that redistributes the applied load over a wider area (Pokharel *et al.* 2010; Leshchinsky 2011; Dash 2012; Thakur *et al.* 2012; Tafreshi *et al.* 2014). It was also reported that a geocell system is a superior form of reinforcement compared to planar geogrid due to its confinement effect (Dash 2004).

The discrete element method introduced by Cundall and Strack (1979) has been used to study the mechanical behaviour of ballast aggregates (McDowell *et al*. 2006; Cui and O'sullivan 2006; Tutumluer *et al*. 2012; Huang and Tutumluer 2011). The DEM provides better insight into the micromechanical behaviour of granular materials such as particle shape, inter-particle movement, particle breakage, and contact force chains developed

between particles that cannot be examined experimentally (McDowell and Harireche 2002; Lobo-Guerrero and Vallejo 2005; Cui and O'sullivan 2006; Bhandari and Han 2010; Indraratna *et al*. 2013; Indraratna *et al*. 2014). The use of DEM to model the mechanical behaviour of sub-ballast aggregates subjected to cyclic train loading is limited in the literature. Lu and McDowell (2010) adopted DEM to model fresh ballast subjected to 100 load cycles and stated that the DEM approach can capture the behaviour of ballast with results that are comparable with 500,000 cycles in an experiment. Bertrand et al. (2005) proposed a DEM model to study the mechanical behaviour of geo-composite cells wrapping an assembly of rocky blocks, capturing the axial force-displacement response of rocky particles as measured in the laboratory. Bhandari and Han (2010) performed two-dimensional DEM analysis and used uniform particles of circular shape to model geotextile-reinforced soils subjected to 25 load cycles. Indraratna *et al*. (2010) simulated fresh ballast in DEM subjected to 1,000 load cycles to capture the behaviour of fresh ballast in terms of the contact force chain and particle breakage mechanisms. Ngo *et al*. (2014) used DEM to study the behaviour of geogrid stabilised ballast fouled with coal, and concluded that the interlocking of ballast aggregates with geogrid was the main reason for the enhanced performance of a ballast assembly stabilised with geogrid. There has been very limited past DEM studies on the behavior of geocell reinforced ballast subjected to a high numbers of load cycles and varied frequencies. Lobo-Guerrero and Vallejo (2006) used a two-dimension discrete element method (DEM) to study the effect of particle crushing, considering a ballast bed subjected to cyclic loads. Ballast aggregates were modelled as idealized circular disks with identical sizes, and the DEM simulation indicated that the induced permanent deformation considerably increased when particle breakage was considered. However, in this study, the loading was limited to 200 cycles and the role of angularity in view of different shapes and sizes of ballast aggregates was not discussed in

detail. Lobo-Guerrero and Vallejo (2010) conducted DEM simulations of model tests for the ballast layer subjected to a total of 425 load cycles. These simulation results showed that stone-blowing was very effective while the use of geosynthetics was found to be less beneficial. This is because the DEM study conducted by Lobo-Guerrero and Vallejo (2006; 2010) employed circular bonded particles, and the simulations were limited to only a few hundred load cycles.

In this paper, the experimental tests were carried out and the discrete element method was used to model geocell-reinforced sub-ballast subjected to cyclic train loading, capturing the deformation and corresponding micro-mechanical characteristics of this composite assembly. The current DEM analysis was able to include irregular shapes of particles to better represent the role of angularity, whereby up to 10,000 load cycles could be performed with different frequencies, and in this respect the current study is an original attempt to capture the more realistic behaviour of the plastic deformation of geocell-reinforced sub-ballast over a much longer cyclic loading duration.

Experimental study

Track Process Simulation Apparatus (TPSA)

A novel track process simulation apparatus (Indraratna and Salim 2005) was modified to study the effect of geocell on the settlement and lateral displacement of sub-ballast. A 800 mm long × 600 mm wide × 450 mm high track process simulation apparatus (TPSA) was fabricated to carry out the model tests, simulating a more realistic sub-ballast layer under rail track, as shown Figure 1. The TPSA was designed to replicate an influence zone, or a unit cell area for a standard gauge Australian track, as illustrated in Figure 2. The four walls of the TPSA were connected with a system of ball bearings and hinges which enabled them

to be either fixed or move laterally at minimum resistance. The specimen was allowed to move in the direction of minor principal stress, σ_3 or parallel to a rail sleeper (e.g., the walls AD and BC in Figure 2 are moveable, $\varepsilon_3 \neq 0$). To simulate a plane strain condition ($\varepsilon_2 = 0$) lateral movement of the specimen in the direction of intermediate stress (σ_2) was restricted by preventing the vertical walls (AB and CD) from moving, thus, mimicking field conditions.

Materials Tested

The sub-ballast used in this study was collected from Bombo quarry near Wollongong, Australia, then cleaned and sieved according to AS 2758.7 (Australia Standards 1996). The particle size distribution of the sub-ballast had an average particle size d_{50} = 3.3 mm, which is similar to current Australian practices in the states of Queensland and New South Wales. The 150mm high geocell with a nominal cellular area of 46x10^3 mm^2 that was used in this study was manufactured from strips of polyethylene polymer that were welded at the joints to create a three-dimensional cellular form. The geocell had a tensile strength for the bulk material and welded section of 9.5kN/m and 8.0 kN/m, respectively, according to ASTM D4885 (ASTM 2011a) and ASTM D4437 (ASTM2013); and its properties are presented in Table 1.

Test Procedures

Sub-ballast aggregates were placed into the apparatus and compacted in sub-layers, each sub-layer was 50mm thick to represent a field density of approximately 2,100 kg/m^3 (relative density ≈ 77%). They were placed and compacted until they were almost 300mm thick, and then a geocell (consisting of 8 cells) was placed on top of the compacted sub-ballast layer. The same aggregates were placed and compacted in an individual geocell

pocket until the sub-ballast was 450mm thick. A cyclic load was generated by a servo hydraulic actuator and transmitted through the sub-ballast by a wooden sleeper connected to a steel rail. In order to simulate a 30 tonne axle load, an average mean stress of 104 kPa was applied onto the sub-ballast assembly. Subsequently, a harmonic cyclic loading with maximum and minimum amplitudes of 166 kPa and 41 kPa, respectively was applied.

During testing, the pressure was controlled using hydraulic jacks connected to the load cells. The experimental program conducted in this study is presented in Table 2, where sub-ballast with and without geocell inclusion was tested under different confining pressures and varying frequencies. Tests without geocell were conducted under three different confining pressures (5-15 kPa) and frequencies (10-30 Hz) while tests with geocell were conducted under confining pressure of 10 kPa and frequencies varying between 10-30 Hz. The confining pressure was equivalent to confinement provided by the weight of the crib and shoulder ballast in the actual track measurements (Indraratna *et al*. 2011a). All tests were carried out with up to 500,000 load cycles. A frequency of 10 Hz was selected based on the freight lines operating in the proximity of V=75 km/h in NSW, Australia, while frequencies of 20 Hz and 30 Hz were approximately selected for increased train speeds of V=145 km/h and V=220 km/h, respectively. Vertical and lateral movements were recorded using an array of settlement plates and electronic potentiometers instrumented at various locations. The results of these tests were used to calibrate and validate the discrete element model presented in the following sections.

DEM simulation of the TPSA

2D modelling of the TPSA

Owing to the configuration of the geocell, three-dimensional modelling of DEM would be required to fully capture realistic load-deformation behaviour between geocell and sub-ballast, and such an analysis often requires extensive input parameters and substantial computational resources. To overcome this limitation, a simplified 2D discrete element analysis was implemented to understand the interaction between geocell and sub-ballast, given that the model was calibrated properly. In this study, an equivalent two-dimensional plane strain model was used in DEM to simulate sub-ballast where the longitudinal strain (ε_2) in the field was almost negligible (Figure 2). The TPSA was simulated in 2D where the dimensions of the DEM model (800 mm x 450 mm) remained the same as the dimensions of test apparatus carried out in the laboratory (Figure 3). The left and right vertical walls were divided into six equal parts, 75mm high; these parts can displace independently in a horizontal direction to simulate the non-uniform lateral spreading of sub-ballast in the tracks, and the variations of lateral displacement with depth can be captured. A specified confining pressure (σ_3) was applied to the left and right walls using a servo control (Itasca, 2008) to maintain the confining pressure. Displacement along the bottom boundary was restrained horizontally and vertically (representing the bottom of the apparatus). A total of 26567 particles, with sizes ranging from 0.5 to 19 mm, were generated to simulate actual sub-ballast gradation with a representative field density of approximately 2,100 kg/m^3. Particles were generated in the assembly at random orientations to resemble experimental conditions. Subroutines were developed to apply cyclic loading characteristics similar to laboratory conditions (q_{max} =166 kPa and q_{min}=41 kPa). The assembly was then cycled to

reach equilibrium (i.e., the ratio of maximum unbalanced force to the mean contact force was smaller than a set tolerance of 10^{-4}) and facilitate the particles to form contacts with each other while keeping the void ratio of the assembly constant.

Determination of micromechanical parameters for sub-ballast

One of the main difficulties of DEM is to select micromechanical parameters so that the behaviour of the resulting material resembles that of the intended physical material. For continuum model, the input properties are often derived directly from measurements performed on laboratory specimens, whereas for DEM, the macroscopic behaviour derives from the micromechanical properties, which are usually unknown **(**Potyondy *et al.* 2004**)**. In this study, micromechanical parameters of sub-ballast were selected by calibrating the load-settlement response obtained from DEM simulations with the tests conducted with sub-ballast alone. The schematic DEM model used in the calibration to model the TPSA for sub-ballast subjected to confining pressures of 5kPa, is presented in Figure 3. The angular-shaped grains of sub-ballast were simulated by connecting several circular-shaped particles together, as illustrated in Figure 4. Within the limitations of plane strain modelling conducted in this study, a simulated 2-D projection of a sub-ballast grain was then assumed to represent a real sub-ballast particle. The shear and normal contact stiffness values selected in the current analysis were based on the process of calibration of DEM results with the experimental data. It is noted that it may not be always realistic to set the normal contact/bond stiffness (k_n) equal to the shear contact/bond stiffness (k_s). However, in this particular analysis the authors have found an acceptable agreement between the DEM simulation and the laboratory results by setting $k_n=k_s$. Moreover, several past studies have also followed the same approach where the ratio of $k_n/k_s=1$ was assumed and acceptable predictions could be derived (e.g. Lim and McDowell (2005); Lobo-Guerrero and Vallejo

(2006); McDowell et al. (2006); Thakur et al. (2010)). It was found that an inter-particle coefficient of friction, μ was a parameter sensitive enough to provide a realistic load-settlement response of sub-ballast. Therefore, the values of μ ranging from 0.60, 0.66, 0.72, and 0.80, were varied during the calibration process. DEM simulations were conducted up to 10,000 load cycles and were carried out at frequencies of 10 Hz. The input parameters were varied interactively until the simulation results matched the laboratory test data. Figure 5 shows comparisons of load-settlement responses obtained from the simulations with the experiment data for different inter-particle coefficients of friction. As expected, an increase of the inter-particle coefficient of friction, μ exhibited a decrease in settlement. The simulation with μ=0.72 resulted in a good agreement with data measured experimentally. A set of micromechanical parameters selected to model sub-ballast is shown in Table 3.

To validate the parameters adopted for sub-ballast, additional DEM simulations were carried out to simulate the load displacement behaviour of sub-ballast subjected to a confining pressure of 15 kPa and cyclic load frequencies of 10 Hz and 20 Hz. The simulated settlement-load cycle curves were compared to the experimental results, as shown in Figure 6. Results obtained from the two simulations agreed reasonably well with the laboratory data, indicating that the parameters presented in Table 3 were reliable. It is also noted that the comparison of 2D DEM simulation with 3D has always been a subject of debate. However, in this study we are considering a 2D Plane Strain condition, which is 3D but with zero strain in the longitudinal direction. In other words, along a straight track, the displacement of sub-ballast along the direction of train passage could be considered insignificant compared to the transverse direction (parallel to sleepers). In the laboratory, 2D plane strain condition was ensured by restraining the two sides in the longitudinal direction (ε_2=0), as shown in Figure 2, while the two sides in the transverse direction (parallel to

sleepers) were allowed to move laterally ($\varepsilon_3 > 0$). Therefore, the Authors believe that the comparison of 2D DEM simulations with the experimental data used in this study is justified, in lieu of a 3D analysis.

Determination of micromechanical parameters for geocell

Modelling geocells has always been a challenging task due to its complex 3D honeycomb structure. Within the scope of this study, the actual three-dimensional form of a geocell was simplified to a two-dimensional projection to facilitate the execution of PFC2D-DEM (plane strain) analysis. A string of continuously connected particles was used in the simulation, as shown in

Figure 7. The geocell pocket structure was simulated by bonding balls of 20 mm-diameter and 10 mm-diameter to form vertical and horizontal panels, respectively. This simplified geocell structure was assumed to be sufficient to provide the confinement effect for the particles packed inside the cellular pockets. Tensile tests were conducted in the laboratory using an INSTRON apparatus (Figure 8a) and by following the Standard D6637, ASTM (2011b). A series of simulated tensile tests were then carried out in DEM to determine the appropriate micromechanical parameters for the geocell by comparing the tensile force-strain response with data measured experimentally. A simplified DEM model of a single geocell pocket was simulated by bonding small circular balls together, as illustrated in Figure 8b. The geocells were secured at one end, while the other end was pulled down with strain increasing up to 6% to obtain the tensile force and strain curve.

While several micromechanical parameters are required to model geocell material, the parallel bond stiffness was a major governing factor considered during calibration. Although the contact bond acts only at the contact and can transmit only normal and shear

forces, a parallel bond acts over a circular cross-section between the two particles in contact, and it can transmit moment (Itasca 2008). The parallel bond may be envisaged as a disk of elastic glue lying on the contact plane where each bond represents the force–displacement behaviour of a finite sized thin element of cementitious material deposited between two circular balls. Relative motion at the contact causes a force and a moment to develop within the parallel bond as a result of its stiffness. A linear contact model (e.g., linear elastic in both the normal and tangential directions) that followed previous studies was used for the current study (e.g. McDowell *et al*. 2006; Ngo *et al*. 2014). In this study, the stiffness of the parallel bond was back calculated based on calibration against tensile tests performed in the laboratory. A series of four simulations with a constant ratio of normal to shear parallel bond stiffness of unity were carried out, while the other parameters remained unchanged. Simulations of the tensile test using DEM to calibrate the parameters for the geocell were limited to the elastic range of maximum strain of 5%, following ASTM Standard D6637. Figure 9 presents comparisons of the tensile load-strain response obtained from the DEM simulations and data measured in the laboratory, and shows that the tensile force-strain response by Simulation 2 agrees well with the test results, indicating that the set of micromechanical parameters used in the simulation given in Table 5 was appropriate.

It is also noted that the honeycomb configuration in geocell acts like a flexible beam embedded in the sub-ballast while simultaneously providing confinement. To examine this effect, additional bending tests were conducted where the geocell was assumed to be a beam with both ends fixed, and having a span of 150 mm, as illustrated in Figure 10a. Each end of the beam was clamped to prevent any movement. The initial load of 10 N was applied at the middle of the beam, and the corresponding mid-span deflection was recorded for reference. The load was increased at a rate of 5 N/minute and the tests were completed at a maximum

load of 140 N. Bending tests with similar loading characteristics were then simulated in DEM, where the beam was modelled by bonding circular balls together and each end was fixed, as shown in Figure 10b. The micromechanical parameters used in the simulation are given in the Table 5. Figure 11 shows comparisons between the experimental data and DEM simulations of the force-deflection responses. It can be seen that the applied load-deflection response in DEM matched the data measured in the laboratory reasonably well, showing that the set of micromechanical parameters used in the simulation are acceptable. Once the given set of micromechanical parameter was calibrated with the test results, they were then used to model a simplified plane strain TPSA of sub-ballast reinforced with geocell, presented in the following sections.

Modelling geocell-reinforced sub-ballast

The DEM model for the plane strain TPSA was used to simulate geocell-reinforced sub-ballast subjected to a confining pressure of $\sigma_3 = 10\ kPa$ and cyclic frequencies of 10, 20, and 30 Hz, similar to the loading conditions implemented in the laboratory. DEM simulations to model the sub-ballast with and without geocell inclusions were conducted up to 10,000 load cycles. The simulated geocell was modelled by contact and parallel bond (

Figure 7) and then positioned into the assembly at the upper portion of the apparatus, as illustrated in Figure 12. The DEM model was cycled until equilibrium was achieved, facilitating the interlock and confinement between the geocell and sub-ballast aggregates. The relatively low time step of 1.15 x 10^{-5} per second was used because it would not unduly disturb the assembly, but it would still attain an acceptable convergence rate, e.g., approximately 182 hours to simulate unreinforced sub-ballast and approximately 236 hours to simulate a geocell-reinforced assembly, using a Dell T7500 workstation. During loading,

vertical displacement of the top wall and lateral movements of the left and right walls were recorded to determine the associated settlements and lateral displacements at corresponding load cycles.

Results and Discussion

Average settlement of sub-ballast with and without geocell inclusion

The average accumulated settlement at varying numbers of load cycles obtained from DEM analysis compared to the laboratory data are presented in Figure 13. It is seen that the results obtained from DEM simulations agreed reasonably well with the experimental data at any given frequency. The predicted and measured results showed that the average settlement increased with an increase in frequency for the unreinforced and reinforced sub-ballast specimens. Generally, the settlements of geocell-reinforced sub-ballast were less than those of the unreinforced assembly. Undoubtedly, this is a result of additional confining pressure induced by the geocell would reduce the sub-ballast settlement. Indeed, when the sub-ballast aggregates were compacted over a geocell, they were confined and projected through the geocell pockets and created a strong mechanical interlock and confinement. This confinement effect enabled the geocell to act as a non-displacement boundary that restrained the sub-ballast grains from free movement, which then decreased the overall settlement. Moreover, the average settlement increased significantly during the first few thousand cycles due to initial particle rearrangement (i.e., the unstable zone), but it increased at a diminished rate in the subsequent load cycles beyond the unstable zone, and approached an approximately constant rate at very high load cycle, N where the sub-ballast aggregates were compressed into a threshold packing arrangement. This observation is in accordance with

studies measured in the laboratory and reported elsewhere by Trani and Indraratna (2010); Indraratna *et al.* (2014); Tafreshi *et al.* (2014).

Lateral deformation of sub-ballast with and without geocell inclusions

Figure 14 shows comparisons between the average lateral deformation (parallel to the sleeper) of sub-ballast from DEM simulation and those measured experimentally, and show that a reasonable match between them was generally obtained. The lateral deformation of sub-ballast increased with an increase in the frequency and then approached a diminishing rate at very high load cycles. Undoubtedly the geocell decreased lateral deformation of the sub-ballast specimens at a given frequency significantly because it confined the sub-ballast and created a stiffened zone that reduce any lateral movement.

Figure 15 shows the variations of lateral displacements of sub-ballast with depth at frequencies of 10 Hz, 20 Hz, and 30 Hz obtained from DEM simulations, and these were based on the tracking positions of wall vertical panels simulated in the DEM analysis (Figure 12). Compared to the unreinforced assembly, the geocell-reinforced sub-ballast experienced less lateral deformation at any given depth and frequency (i.e. for a given frequency of 20 HZ and a depth of 300mm, the unreinforced assembly exhibited a lateral displacement of 21.6 mm compared to 14.2 mm for the reinforced case). Lateral spreading started from the top surface of the sub-ballast and increased considerably up to a depth of 300mm below the surface. Below a depth of 300mm, lateral displacement began decreasing due to a non-movement boundary at the bottom of the TPSA. The laboratory and simulation results indicated that geocell decreased settlement and substantially reduced the sub-ballast from spreading laterally.

Contact force distributions of geocell-reinforced sub-ballast

Forces in a granular assembly are transferred through an interconnected network of force chains via contact points. Taking an advantage of a DEM simulation, the contact force chains of sub-ballast and geocell were captured. Figure 16a illustrates the contact force distributions of an unreinforced sub-ballast assembly at a settlement (S) of 5 mm, while Figures 16b-d show the contact force distributions of geocell-reinforced sub-ballast at settlements of S=5 mm, 15 mm, and 20 mm, respectively, subjected to the cyclic load at a given frequency of 20 Hz. The contact forces between the particles were plotted as lines on the same scale, whose thickness was according to their magnitudes. The black lines indicate compressive contact forces and the red lines indicate tensile contact forces. For the sake of clarity, only those contacts with a magnitude exceeding the average force of the whole assembly were plotted. They clearly show that the total number of contact forces and maximum contact forces increased as settlement increased, mainly because the assembly was compacted and compressed to sustain the external load, which in turn increased the quantity and magnitude of the contact forces. For example, with reinforced sub-ballast, the number of contacts was 60,252 at a settlement of 5 mm, and it increased to 78,252 and 83,521 contacts for settlements of S=15 and 20 mm, respectively. The maximum contact forces also increased with an increase of settlement, and these were 745 N, 857 N and 946 N at the settlements of S=5, 15 and 20 mm, respectively. Compared to the unreinforced sub-ballast (Figure 16a), the reinforced assemblies created more contacts within the geocell regions, and this would be attributed to the confinement the geocell induced to the grains of sub-ballast. It can also be seen that the tensile forces in geocells are mobilised with an increased in settlement.

Figure 17 shows the variations of average normal contact and shear forces with depth at the end of tests for reinforced and unreinforced sub-ballast assemblies. Compared to the unreinforced assemblies (Figures 17c, 17d), geocell induced a significant increase in the contact forces within this region, but underneath the geocell the average normal and shear contact forces decreased with depth and approached almost constant values near the bottom of the assembly of the reinforced and unreinforced specimens. Undoubtedly the inclusion of geocell reduced the shear and normal contact force in sub-ballast below the geocell. It is worth mentioning that the micro-mechanics of the geocell-reinforced sub-ballast conducted in this study was limited to the distribution of contact force chains and the average contact normal and shear force distributions. However, the comparison of the experimental observations with the 2D plane strain DEM analysis proves that to the current analysis was able to capture the load-deformation behaviour of geocell-stabilised sub-ballast in spite of these limitations. Naturally, the authors have made a few simplifications to keep the micro-mechanical analysis fairly simples, as the requirements of brevity of this manuscript would not allow the reporting of more detailed DEM analyses that could capture other micro-mechanical aspects such as the evolution of fabric anisotropy and complex detailing of changing angularity with the high number of loading cycles.

Conclusions

A large-scale Track Process Simulation Apparatus (TPSA) was used to carry out on sub-ballast with and without geocell inclusion, and then the results were used to validate and compare with the DEM simulation. Irregular particles of sub-ballast could be simulated by clumping several circular balls together to represent appropriate angularity. A 2D plane strain DEM model for geocell was developed by bonding small balls together to form the cellular pockets with contact and parallel bonds. Appropriate sets of micromechanical parameters to simulate sub-ballast and geocell were calibrated and selected by comparing laboratory measured load-deformation curves with those predicted by the DEM model. Once the micromechanical parameters were properly validated, they were used to simulate the TPSA for testing sub-ballast at frequencies of 10 Hz, 20 Hz and 30 Hz.

Results of the average vertical settlements and lateral displacements were comparable with experimental data subjected to a given frequency, indicating that the DEM model proposed in this study could capture the load–displacement behaviour of sub-ballast reinforced with geocells. As the frequency increased, the settlement and lateral spreading of sub-ballast of the reinforced and unreinforced assemblies increased, but unlike the unreinforced sample, the geocell-reinforced sub-ballast experienced significantly less deformation. This was undoubtedly attributed to the confinement provided by geocell that prevented particles from 'free' lateral movement that would otherwise occur.

Taking advantage of the DEM simulation, the contact force distributions of geocell-stabilised sub-ballast subjected to a cyclic frequency of 20 Hz was presented. The simulation showed that the total number of contact force chains and the maximum contact force increased with an increase in settlement, and this was attributed to the granular

assembly compressing under the applied cyclic load. The average contact normal and shear forces developed inside the model at varying depths were also presented. The magnitudes of these forces within the geocell zone were significantly greater than the other locations, primarily due to the mobilisation of large contact forces between the geocell and sub-ballast. Underneath the geocell, the average normal and shear contact forces decreased with depth and approached almost constant values near the bottom of the granular assembly.

The proposed DEM model could provide a fundamental numerical framework to inspire further studies in relation to sub-ballast reinforced by geocell. Despite the assumptions made for this 2D (plane strain) DEM analysis, the computed results were still adequate for understanding the fundamental deformation behaviour of the geocell-reinforced sub-ballast subjected to cyclic loading.

Acknowledgement

The authors would like to express their appreciation to the Australian Research Council (ARC) for providing funding to this Project.

Nomenclature

d_{50}	medium value of the particle size distribution
k_n	contact normal stiffness
k_s	contact shear stiffness
$k_{n\text{-}wall}$	contact normal stiffness of wall-particle
$k_{s\text{-}wall}$	contact shear stiffness of wall-particle
q_{max}	maximum cyclic load
q_{min}	minimum cyclic load
N	number of load cycle
S	vertical settlement
V	train speed
μ	coefficient of friction
σ_2	intermediate stress
σ_3	confining pressure (minor principal stress)
ε_2	longitudinal strain (strain perpendicular to sleeper)
ε_3	lateral strain parallel to sleeper

References

Anderson, W. F. , and Fair, P. (2008). "Behavior of railroad ballast under monotonic and cyclic loading". *Journal of Geotechnical and Geoenvironmental Engineering, ASCE.* 143(3): 316–327.

Ashmawy, A. K. , and Bourdeau, P. L. (1995). "Geosynthetic- reinforced soils under repeated loading: A review and comparative design study",". *Geosynthetics International.* 2(4): 643-678.

Australian Standard. (1996). "Aggregates and rock for engineering purposes; Part 7: Railway ballast." *AS 2758.7*. Sydney, Australia.

ASTM. (2010). "Standard test method for density of plastics by the densitygradient technique." *D1505-10*, West Conshohocken, PA.

ASTM. (2011a). "Standard test method for determining performance strength of geomembranes by the wide strip tensile method." *D4885-01(2011)*, West Conshohocken, PA.

ASTM. (2012). "Standard test method for measuring the nominal thickness of geosynthetics." *D5199-12*, West Conshohocken, PA.

ASTM. (2013). "Standard practice for non-destructive testing (NDT) for determining the integrity of seams used in joining flexible polymeric sheet geomembranes." *D4437-08(2013)*, West Conshohocken, PA.

ASTM. (2011b). "Standard test method for determining the tensile properties of geogrids by the single rib or multi-rib tensile method". *D6637*. Philadelphia, USA; 2011

Bathurst, R. J. , and Raymond, G. P. (1987). "Geogrid reinforcement of ballasted track". *Transportation Research Record.* 1153: 8-14.

Bhandari, A. , and Han, J. (2010). "Investigation of geotextile-soil interaction under a cyclic vertical load using the discrete element method". *Geotextiles and Geomembranes.* 28(1): 33-43.

Bertrand, D., Nicot, F., Gotteland, P., Lambert, S. (2005). “Modelling a geo-composite cell using discrete analysis". *Computers and Geotechnics.* 32 (8) 564–577.

Cui, L. , and O'Sullivan, C. (2006). "Exploring the macro- and micro-scale response of an idealised granular material in the direct shear apparatus". *Géotechnique.* 56(7): 455-468.

Cundall, P. A. , and Strack, O. D. L. (1979). "A discrete numerical model for granular assemblies". *Géotechnique.* 29(1): 47-65.

Dash, S. (2012). "Effect of geocell type on load-carrying mechanisms of geocell-reinforced sand foundations". *International Journal of Geomechanics.* 12(5): 537-548.

Dash, S. K., Rajagopal, K., Krishnaswamy, K.N. (2004). "Performance of different geosynthetic reinforcement materials in sand foundations". *Geosynthetics International.* 11(1): 35-42.

Fernandes, G., Palmeira, E. M. , and Gomes, R. C. (2008). "Performance of geosynthetic-reinforced alternative sub-ballast material in a railway track". *Geosynthetics International.* 15(5): 311-321.

Giroud, J. P. , and Han, J. (2004). "Design method for geogrid-reinforced unpaved roads. I. Development of design method". *Journal of Geotechnical and Geoenvironmental Engineering.* 130(8): 775-786.

Huang, H. , and Tutumluer, E. (2011). "Discrete Element Modeling for fouled railroad ballast". *Construction and Building Materials*. 25: 3306-3312.

Indraratna, B., Thakur, P. K. , and Vinod, J. S. (2010). "Experimental and numerical study of railway ballast behavior under cyclic loading". *International Journal of Geomechanics, ASCE.* 10(4): 136-144.

Indraratna, B., Biabani, M. , and Nimbalkar, S. (2015) "Behavior of Geocell-Reinforced Subballast Subjected to Cyclic Loading in Plane-Strain Condition". *Journal of Geotechnical and Geoenvironmental Engineering.* 141(1): 1-16.

Indraratna, B., Ngo, N. T. , and Rujikiatkamjorn, C. (2011b). "Behavior of geogrid-reinforced ballast under various levels of fouling". *Geotextiles and Geomembranes.* 29(3): 313-322.

Indraratna, B., Ngo, N. T. , and Rujikiatkamjorn, C. (2013). "Studying the Deformation of Coal Fouled Ballast Stabilised with Geogrid under Cyclic Load". *Journal of Geotechnical and Geoenvironmental Engineering, ASCE.* 139(8): 1275-1289.

Indraratna, B., Ngo, N., Rujikiatkamjorn, C. , and Vinod, J. (2014). "Behavior of Fresh and Fouled Railway Ballast Subjected to Direct Shear Testing: Discrete Element Simulation". *International Journal of Geomechanics*. 14(1): 34-44.

Indraratna, B. , and Salim, W. (2005). Mechanics of ballasted rail tracks - A Geotechnical Perspective, Taylor and Francis. Balkema, London, UK.

Indraratna, B., Salim, W. , and Rujikiatkamjorn, C. (2011a). Advanced rail geotechnology - ballasted track, CRC Press, Taylor & Francis Group, London, UK

Itasca (2008). "Particle flow code in two dimensions (PFC2D)". Itasca Consulting Group, Inc., Minnesota, USA.

Lackenby, J., Indraratna, B., McDowell, G. R. , and Christie, D. (2007). "Effect of confining pressure on ballast degradation and deformation under cyclic triaxial loading". *Geotechnique.* 57(6): 527–536.

Leshchinsky, B. (2011). "Enhancing ballast performance using geocell confinement". *Proceedings of Geo-Frontiers.* 4693-4072.

Lim, W. L. , and McDowell, G. R. (2005). "Discrete element modelling of railway ballast". *Granular Matter*. 7(1): 19-29.

Lobo-Guerrero, S. , and Vallejo, L. E. (2005). "Discrete element method evaluation of granular crushing under direct shear test condition". *Journal of Geotechnical and Geoenvironmental Engineering.* 131(10): 1295-1300.

Lobo-Guerrero, S., and Vallejo, L.E. (2006). Discrete element method analysis of railtrack ballast degradation during cyclic loading. *Granular Matter.* 8(3):195-204.

Lobo-Guerrero S., and Vallejo L.E. (2010). The effectiveness of geosynthetic reinforcement, tamping, and stoneblowing of railtrack ballast beds under dynamic loading: DEM analysis. *Geomechanics and Engineering*. 2(3), 161-171.

Lu, M. , and McDowell, G. R. (2010). "Discrete element modelling of railway ballast under monotonic and cyclic triaxial loading". *Géotechnique.* 60(6): 459-467.

McDowell, G. R. , and Harireche, O. (2002). "Discrete element modelling of soil particle fracture". *Geotechnique.* 52(2): 131-135.

McDowell, G. R., Harireche, O., Konietzky, H., Brown, S. F. , and Thom, N. H. (2006). "Discrete element modelling of geogrid-reinforced aggregates". *Proceedings of the ICE - Geotechnical Engineering* 159(1): 35-48.

Ngo, N. T., Indraratna, B. , and Rujikiatkamjorn, C. (2014). "DEM simulation of the behaviour of geogrid stabilised ballast fouled with coal". *Computers and Geotechnics.* 55: 224-231.

Pokharel, S. K., Han, J., Leshchinsky, D., Parsons, R. L. , and Halahmi, I. (2010). "Investigation of factors influencing behavior of single geocell-reinforced bases under static loading". *Geotextiles and Geomembranes.* 28(6): 570-578.

Potyondy, D. O. , and Cundall, P. A. (2004). "A bonded-particle model for rock". *International Journal of Rock Mechanics and Mining Sciences.* 41(8): 1329-1364.

Selig, E. T. , and Waters, J. M. (1994). Track geotechnology and substructure management, Thomas Telford, London.

Suiker, A. S. J., Selig, E. T. , and Frenkel, R. (2005). "Static and cyclic triaxial testing of ballast and subballast". *Journal of Geotechnical and Geoenvironmental Engineering, ASCE* 131(6): 771–782.

Tafreshi, S. N. M., Khalaj, O. , and Dawson, A. R. (2014). "Repeated loading of soil containing granulated rubber and multiple geocell layers". *Geotextiles and Geomembranes.* 42(1): 25-38.

Thakur, P. K., Vinod, J. S. , and Indraratna, B. (2010). "Effect of particle breakage on cyclic densification of ballast: A DEM approach". *Materials Science and Engineering*. 10: 1-7.

Thakur, J. K., Han, J., Pokharel, S. K. , and Parsons, R. L. (2012). "Performance of geocell-reinforced recycled asphalt pavement (RAP) bases over weak subgrade under cyclic plate loading". *Geotextiles and Geomembranes.* 35(0): 14-24.

Trani, L. D. O. , and Indraratna, B. (2010). "Assessment of subballast filtration under cyclic loading". *Journal of Geotechnical and Geoenvironmental Engineering.* 136(11): 1519-1528.

Tutumluer, E., Huang, H., and Bian, X. (2012). “Geogrid-aggregate interlock mechanism investigated through aggregate imaging-based discrete element modeling approach.” *International Journal of Geomechanics, ASCE*. 12(4): 391–398.

Table 1. Properties of geocell used for the study

Characteristics	Properties	Values / details
Physical	Material	Polyethylene
	Aperture size (length x width) (mm)	302 x 287
	Wall type	Perforated, textured
	Cell wall open area (%)	16.8
	Nominal area (mm^2)	46 x 10^3
	Cell (per m^2)	21.7
	Cell depth (mm)	150
	Weld spacing (mm)	445
	Thickness (mm)	1.3[a]
	Colour	Black from carbon black (1.5-2% by weight)
Technical	Tensile strength for bulk material (kN/m)	9.5[b]
	Tensile strength for seam (kN/m)	8[c]
	Minimum cell seam strength (kN/m)	2.13
	Density (g/cm^3)	0.95[d]

[a]ASTM (2012) - D5199-12
[b]ASTM (2011a) - D4885-01
[c]ASTM (2013) - D4437-08
[d]ASTM(2010) - D1505-10

Table 2. Experimental program

Confining pressure, σ_3 (kPa)	Frequency, *f* (Hz)	Without geocell	With geocell	No. of tests
5	10	X		1
10	10	X	X	2
10	20	X	X	2
10	30	X	X	2
15	10	X		1
15	20	X		1

Table 3. Micromechanical parameter used to simulate sub-ballast

Parameters	Sub-ballast
Particle density (kg/m^3)	2100
Inter-particle coefficient of friction, μ	0.72
Contact normal stiffness, k_n (N/m)	2.56×10^8
Contact shear stiffness, k_s (N/m)	2.56×10^8
Parallel bond normal and shear stiffness (N/m)	5.36×10^9
Parallel bond normal and shear strength (N/m^2)	8.53×10^9
Parallel bond radius multiplier	0.5
Contact normal stiffness of wall-particle, $k_{n\text{-}wall}$ (N/m)	1.5×10^9
Shear stiffness of wall of wall-particle, $k_{s\text{-}wall}$ (Nm)	1.5×10^9

Table 4. Parameters of parallel bonds used to simulate the geocell

	Parallel bond normal stiffness, k_{np} (kPa/m)	Parallel bond shear stiffness, k_{sp} (kPa/m)
Simulation 1	9.72×10^6	9.72×10^6
Simulation 2	4.86×10^7	4.86×10^7
Simulation 3	2.43×10^8	2.43×10^8
Simulation 4	12.15×10^8	12.15×10^8

Table 5.Micromechanical parameters of geocell adopted for DEM simulation

Parameter	Selected value
Particle density (kg/m$^{3)}$	950
Coefficient of friction	0.45
Contact normal stiffness, k_n (N/m)	6.51×10^6
Contact shear stiffness, k_s (N/m)	6.51×10^6
Contact normal stiffness of wall-particle, $k_{n\text{-}wall}$ (N/m)	$1.35x10^8$
Shear stiffness of wall of wall-particle, $k_{s\text{-}wall}$ (N/m)	$1.35x10^8$
Parameter of contact bond normal strength, ϕ_n(kN)	43.2
Parameter of contact bond shear strength, ϕ_s (kN)	43.2
Parallel bond radius multiplier, r_p	0.5
Parallel bond normal stiffness, k_{np} (kPa/m)	4.86×10^7
Parallel bond shear stiffness, k_{sp} (kPa/m)	4.86×10^7
Parallel bond normal strength, σ_{np} (MPa)	352
Parallel bond shear strength, σ_{sp} (MPa)	352

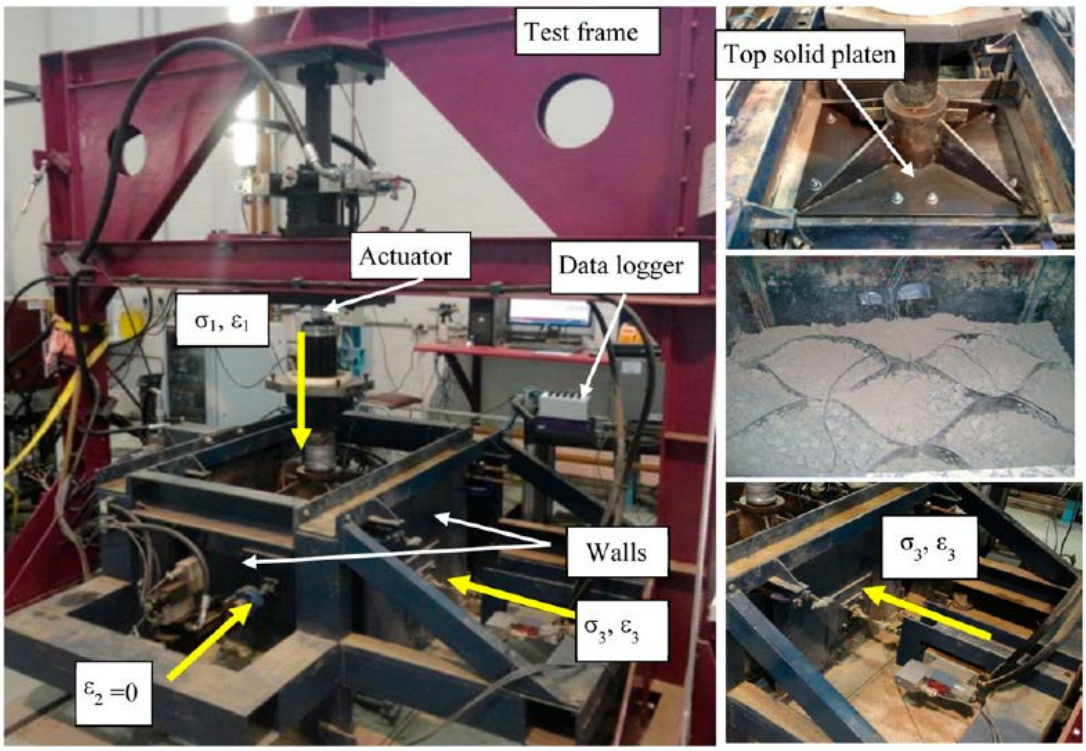

Figure 1. The track process simulation apparatus (TPSA) used for testing of geocell-reinforced sub-ballast (modified after Indraratna *et al.*2015)

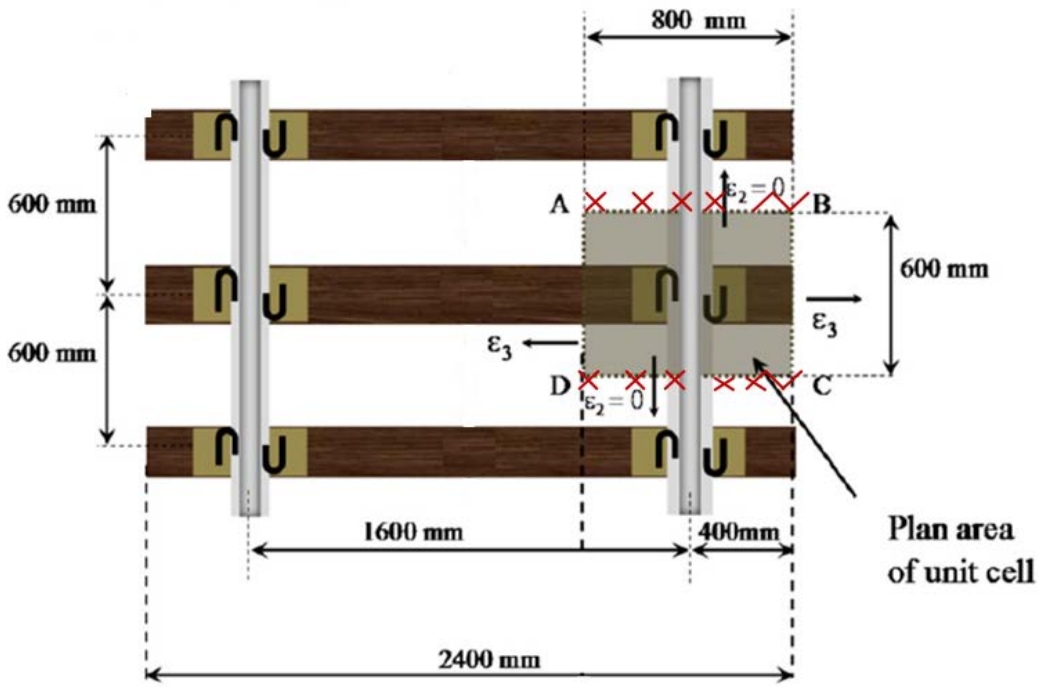

Figure 2.Schematic plan view of the section of track simulated by the laboratory apparatus (modified after Indraratna *et al.*2015)

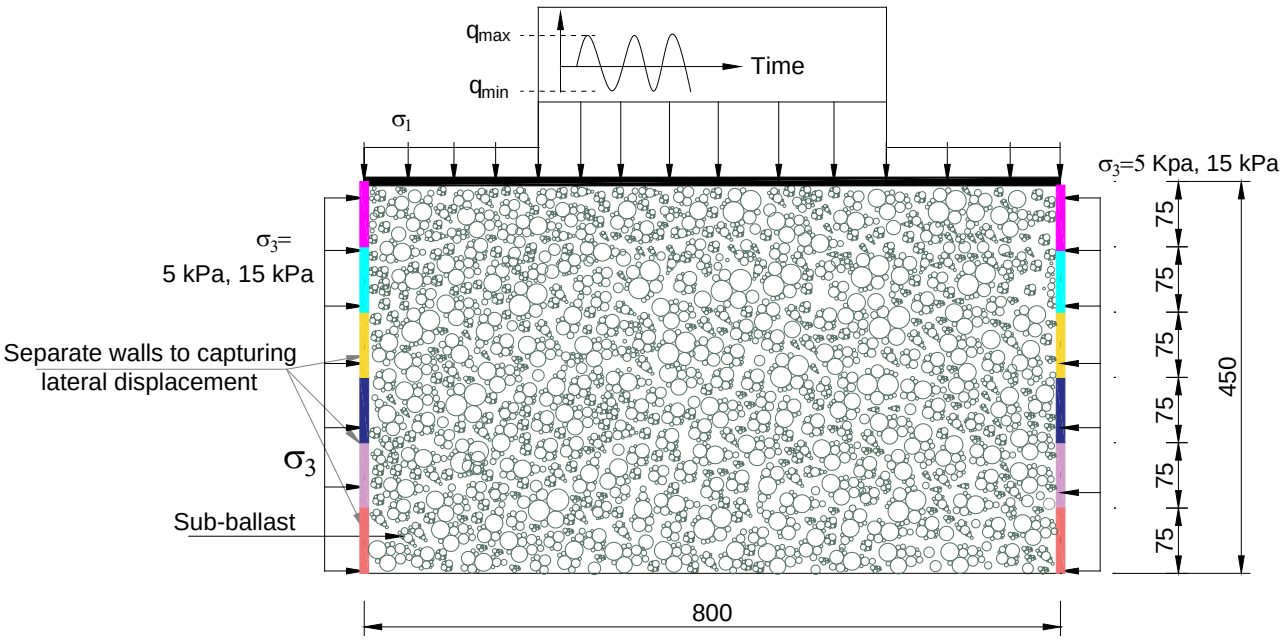

Figure 3. Schematic DEM model used to calibrate sub-ballast micromechanical parameters

(dimensions in mm)

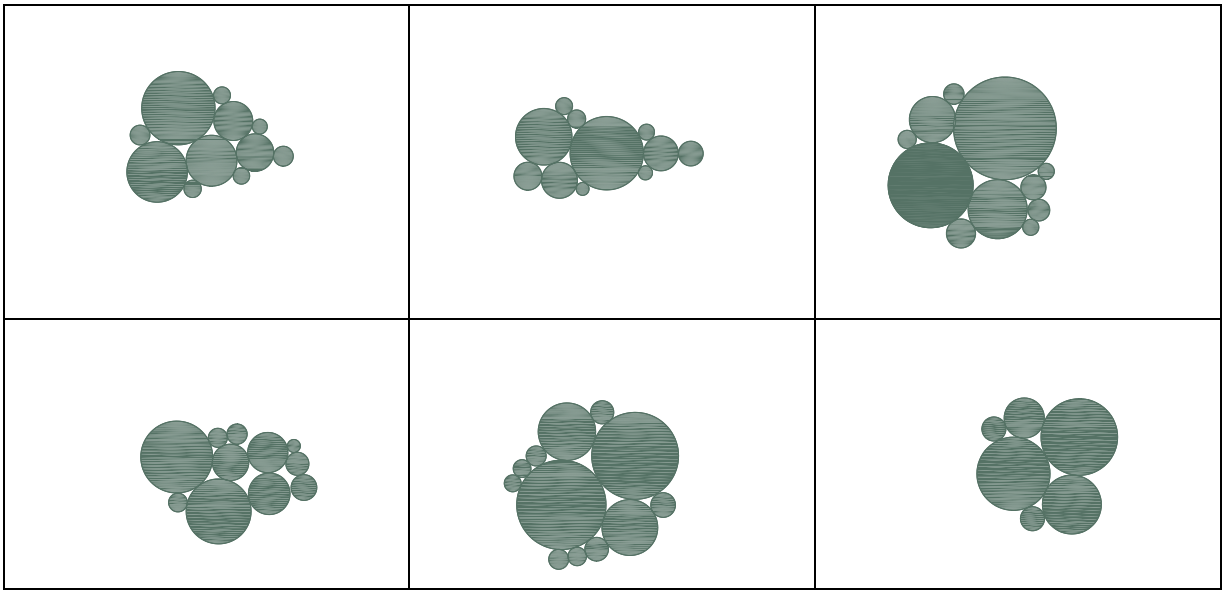

Figure 4. Representative sub-ballast particle shapes used in the DEM simulation

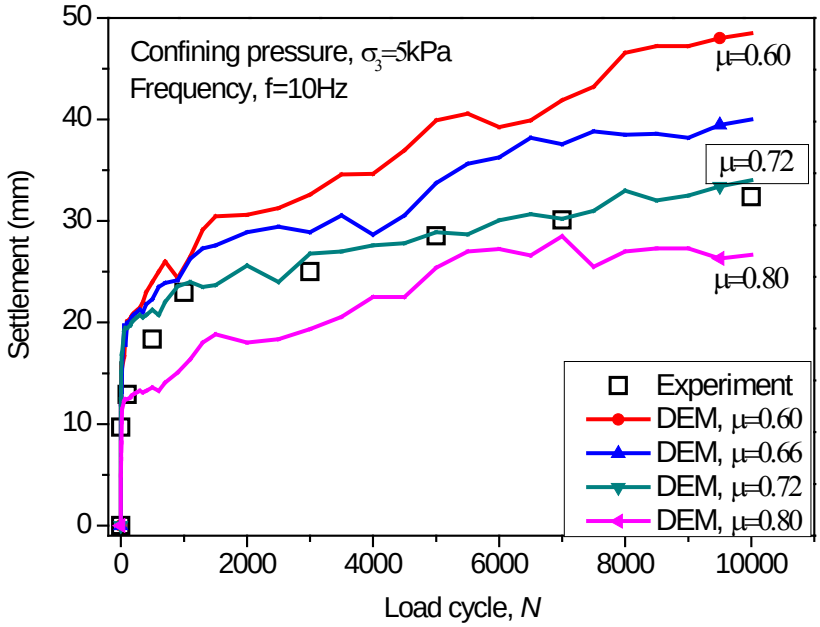

Figure 5. Comparison of settlement-load cycle between DEM simulation and experimental data with varied inter-particle friction.

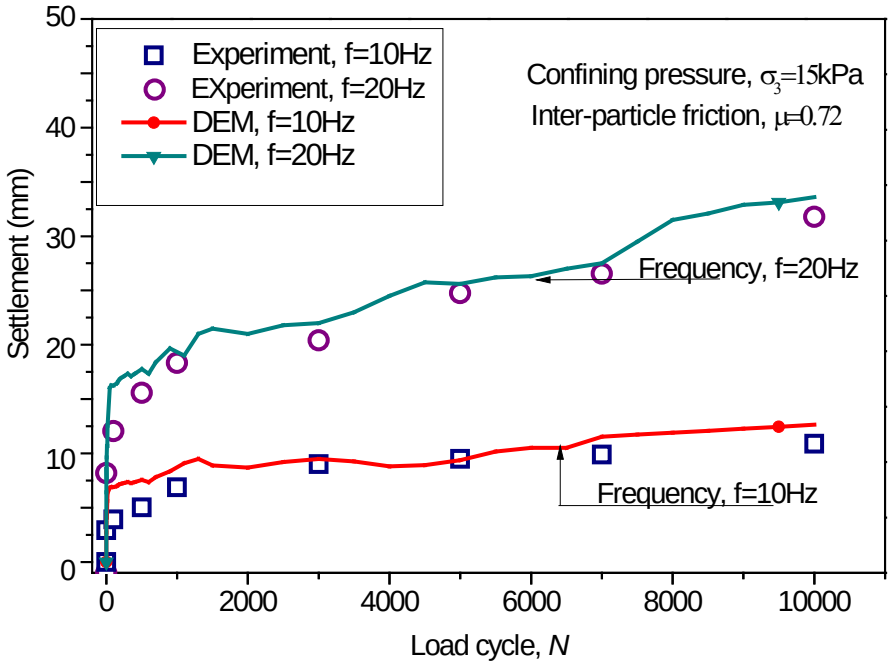

Figure 6. Comparison of settlement-load cycle between experimental data and DEM simulation for μ=0.72, subjected to confining pressure of σ_3=15kPa.

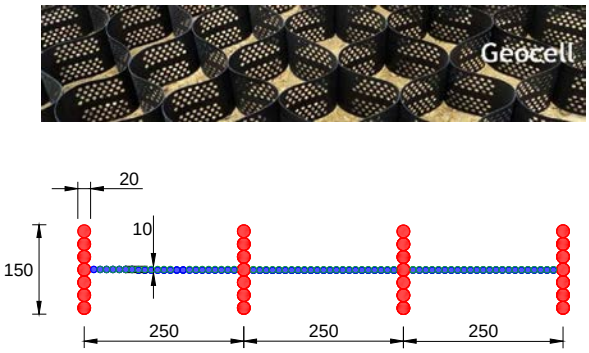

Figure 7. Simplified geocell modelling in DEM (dimensions in mm)

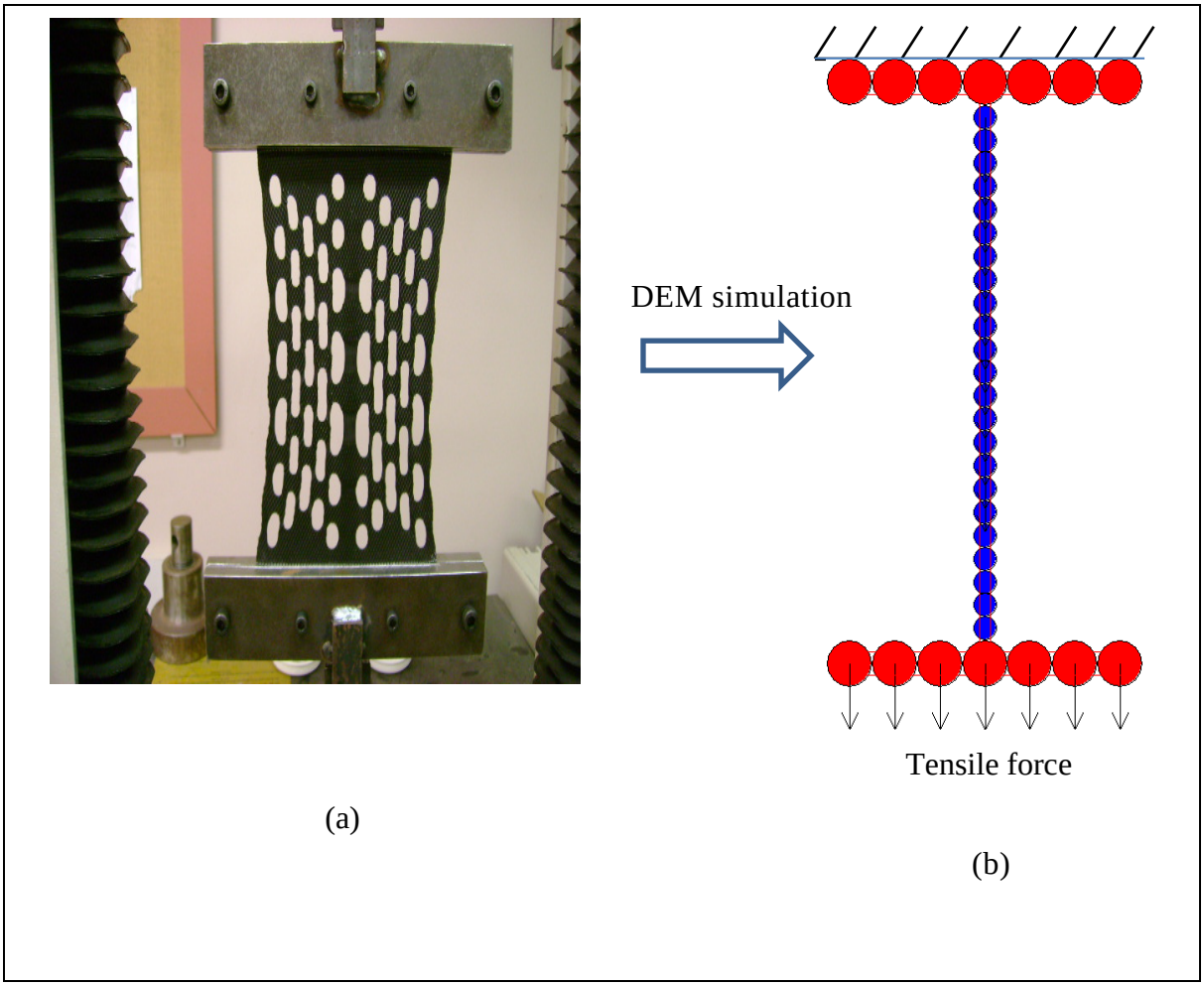

Figure 8. Calibration of geocell: (a) tensile test for geocell; (b) simplified model of a single geocell pocket in DEM

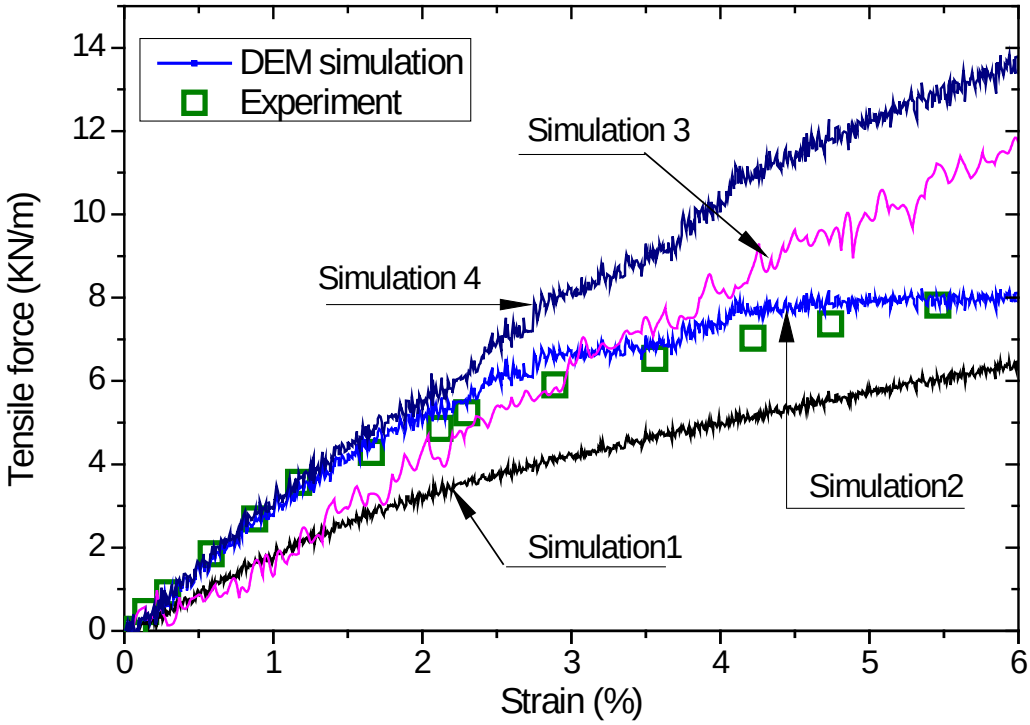

Figure 9. Comparison between the DEM simulations the tensile test results for geocell

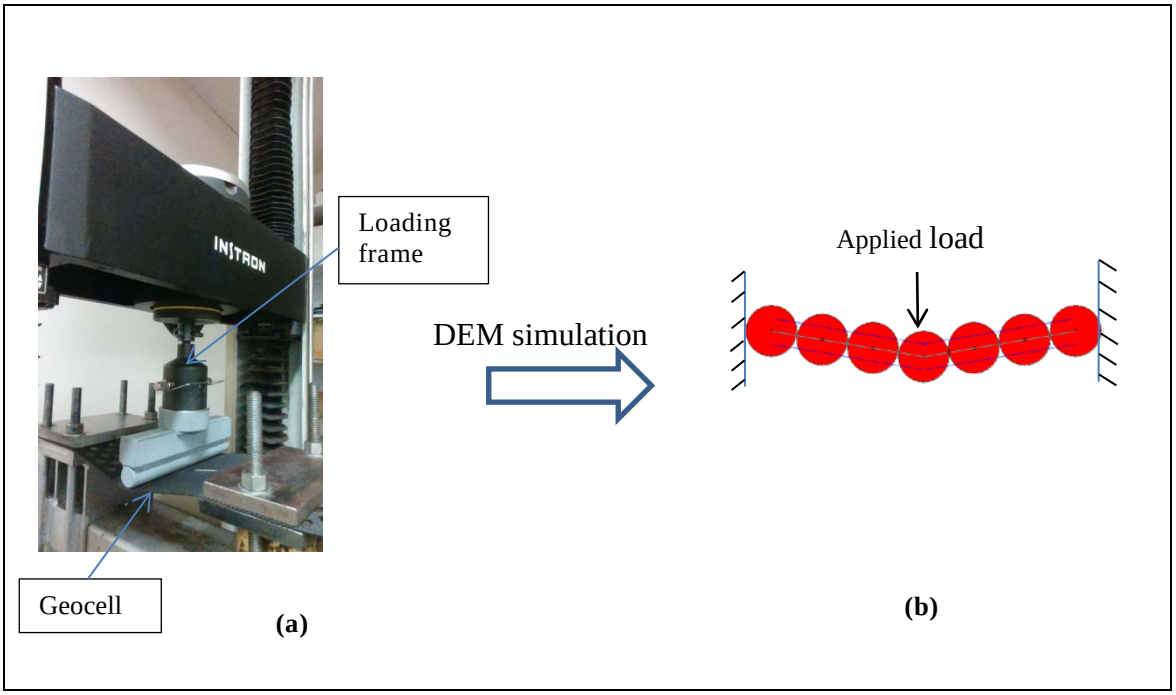

Figure 10. Bending test for geocell: (a) physical bending test; (b) DEM simulation of bending test

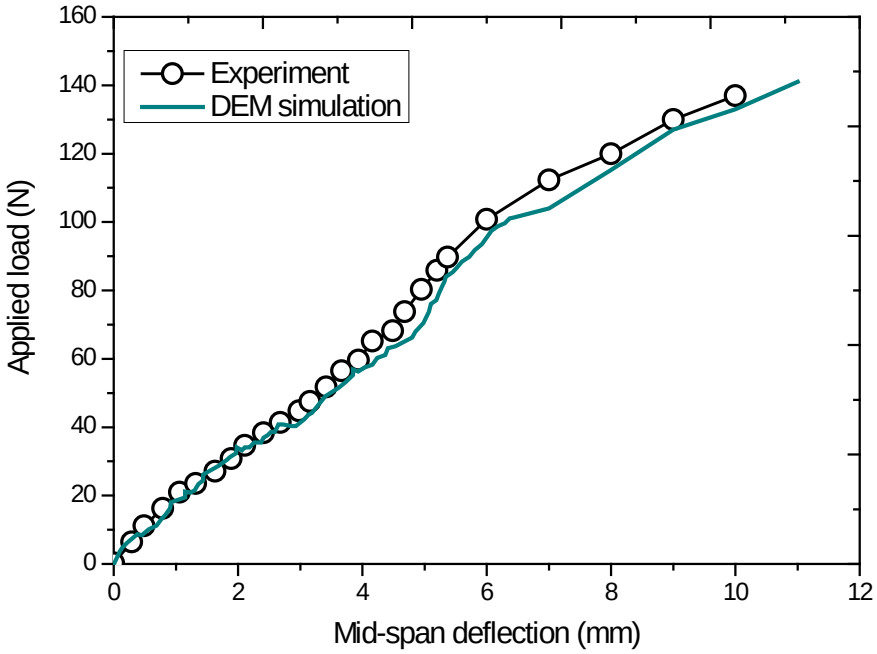

Figure 11. Comparison between the DEM simulations and experiment of the bending test for geocell

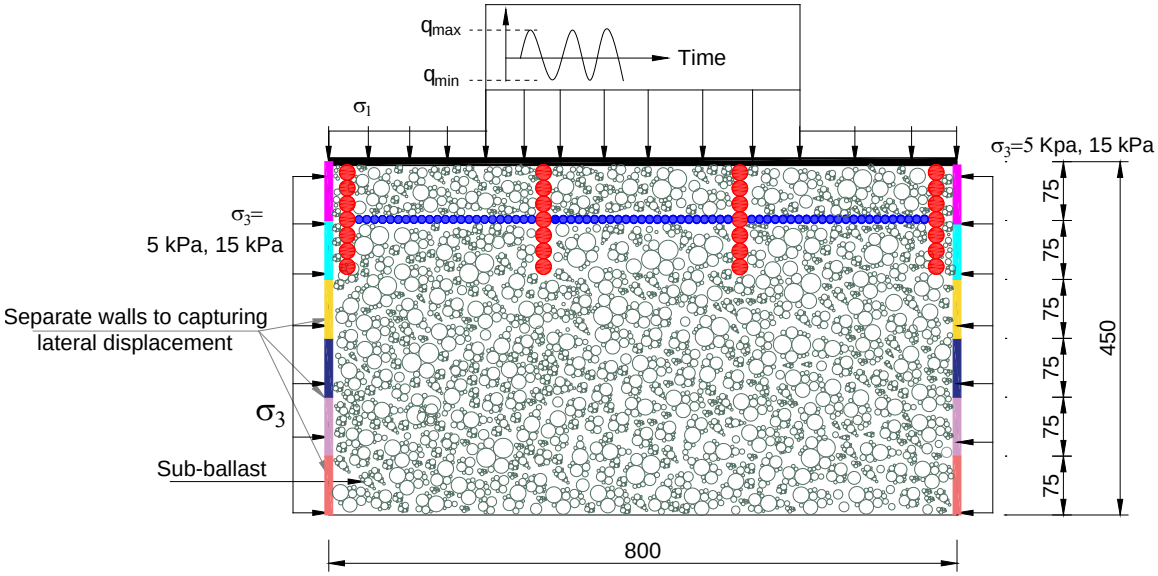

Figure 12. Schematic diagram of plane train modelling for the TPSA for geocel-reinforced sub-ballast (dimensions in mm)

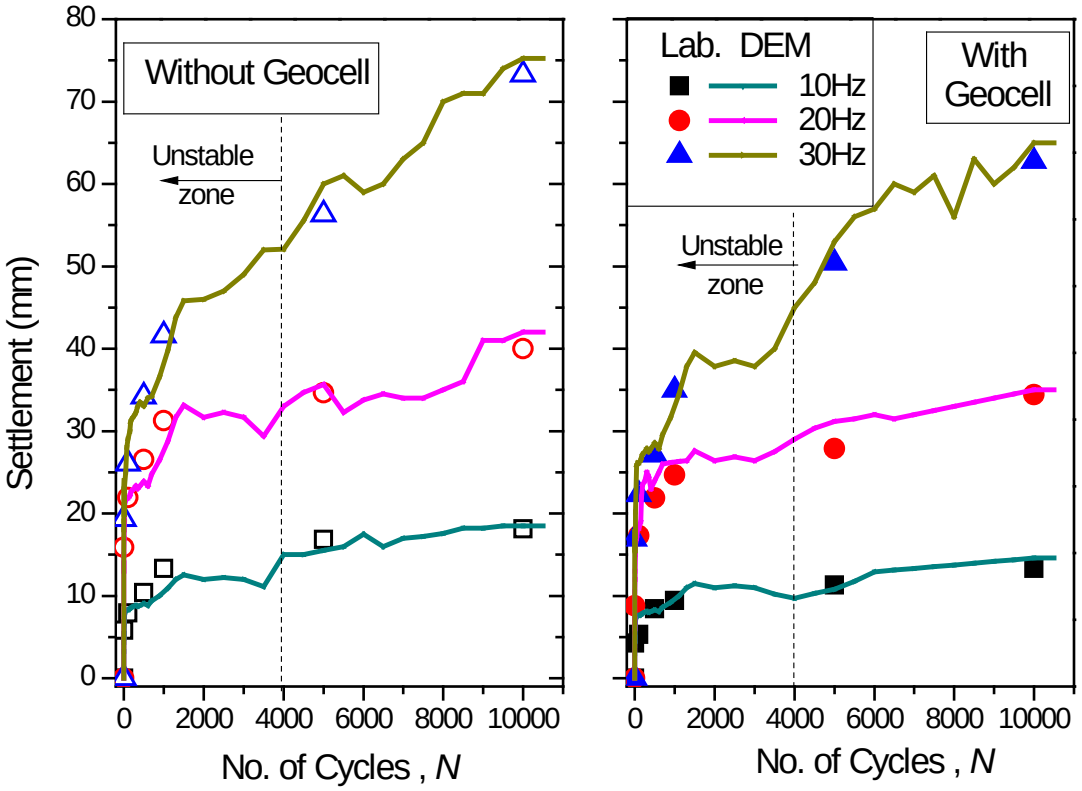

Figure 13. Comparisons of sub-ballast settlement at varying cyclic load cycles, *N* with/without geocell inclusion measured experimentally and predicted in DEM

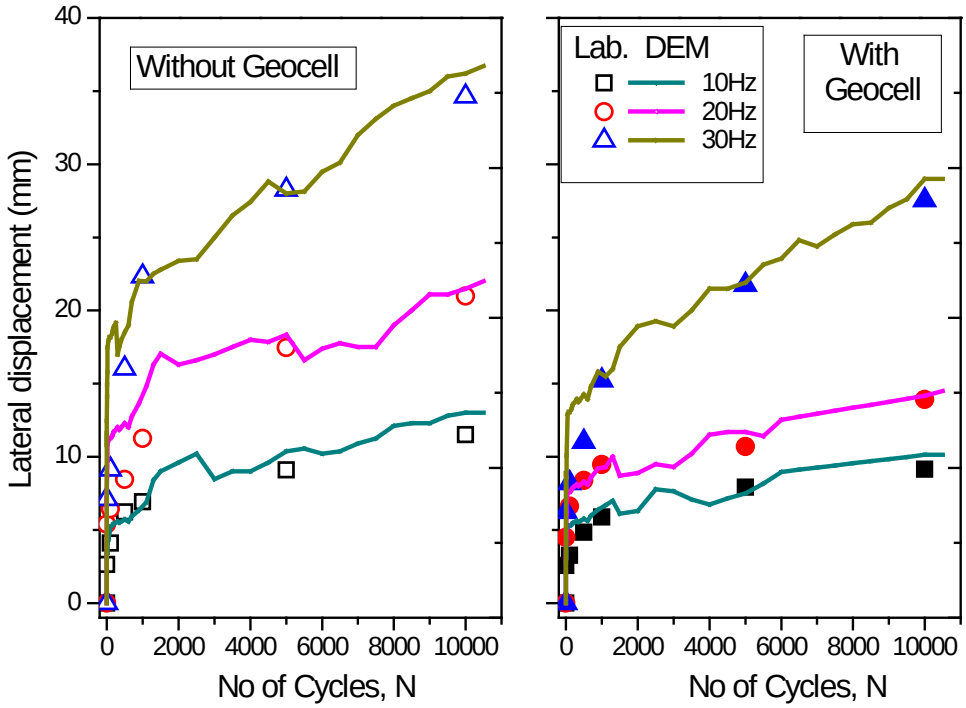

Figure 14. Comparisons of lateral displacement of sub-ballast with/without geocell inclusion measured experimentally and predicted in DEM

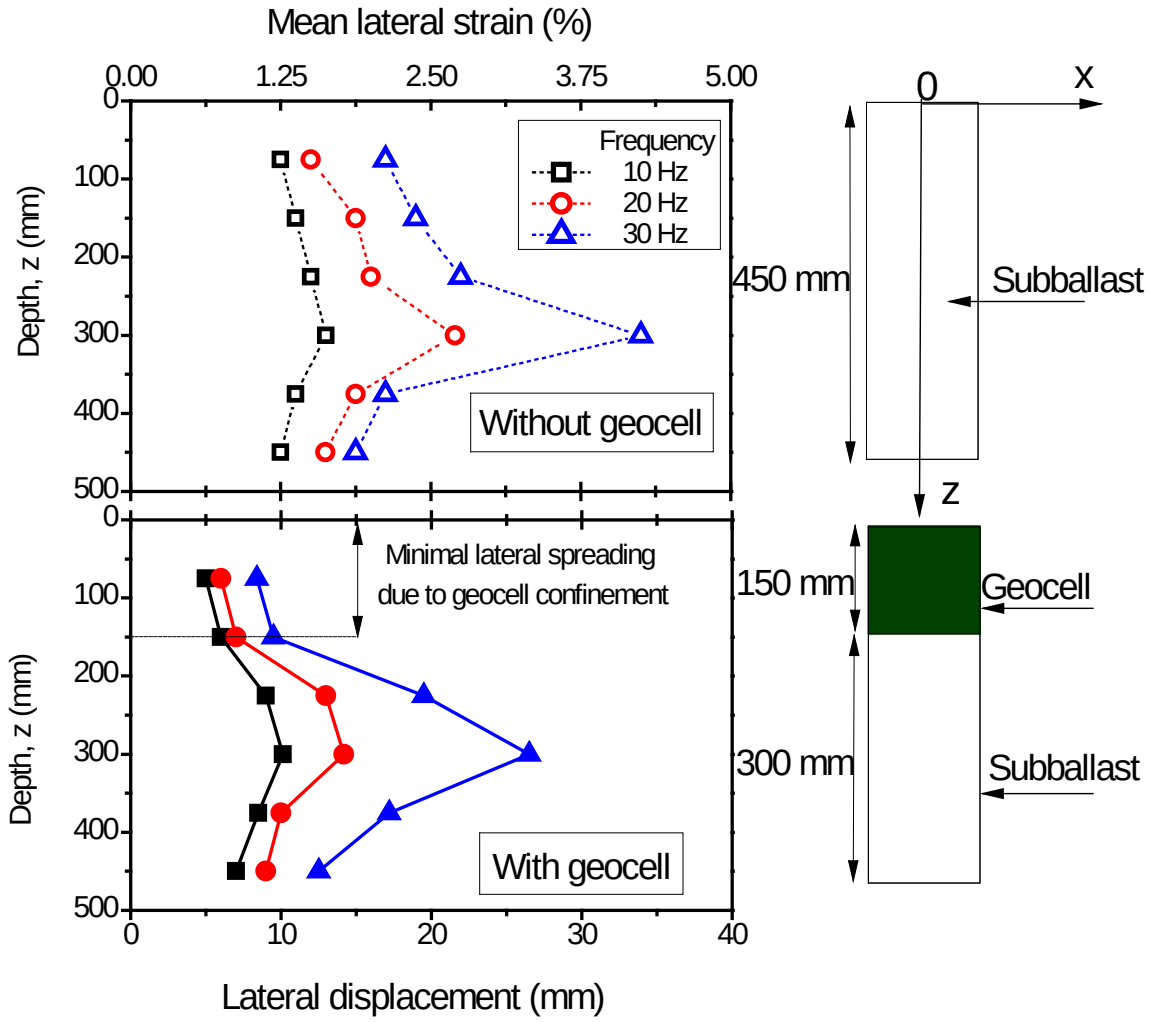

Figure 15. Predicted lateral displacement of sub-ballast with depth

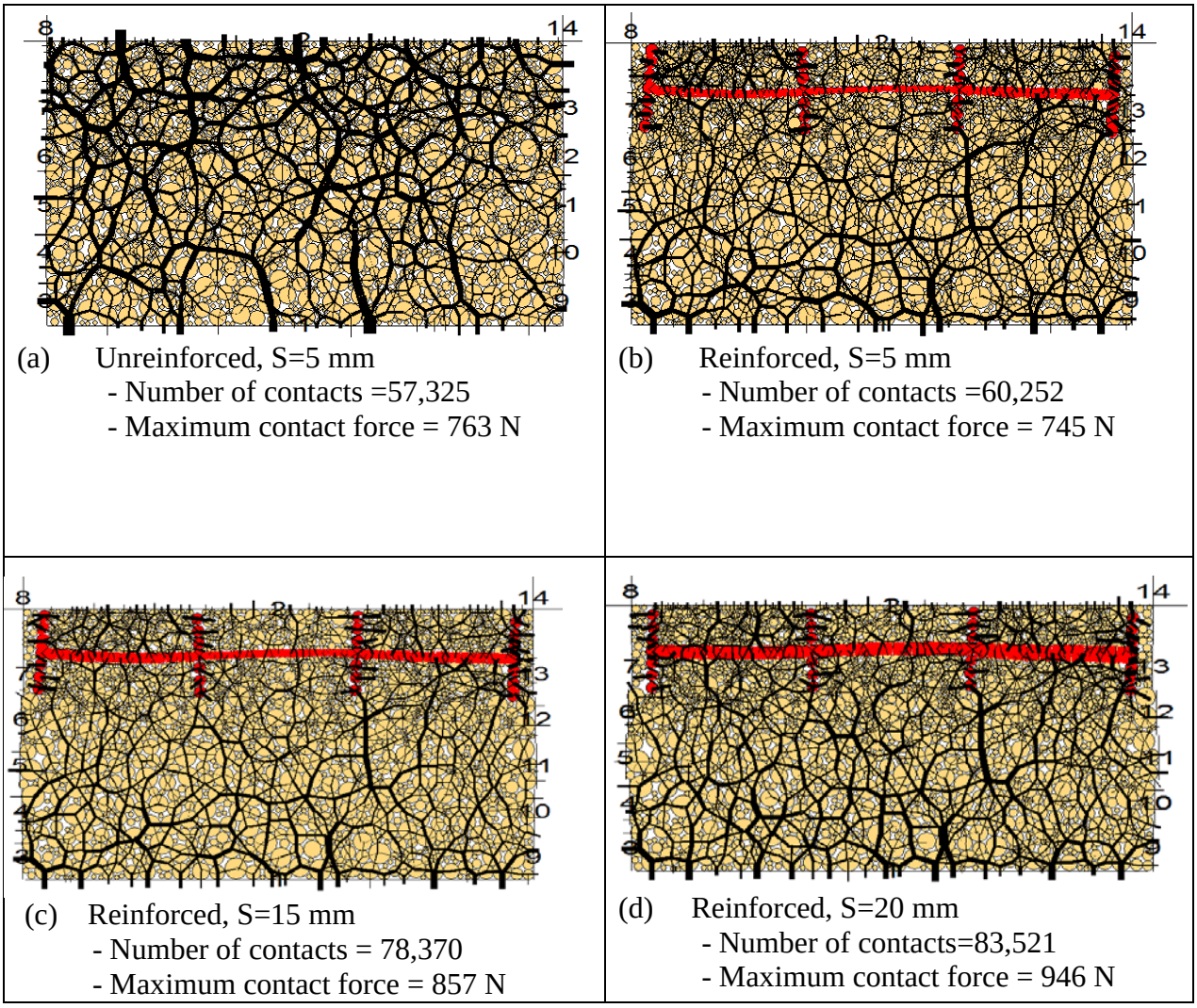

Figure 16. Distribution of contact forces unreinforced/reinforced sub-ballast at different settlements, *S*: (a) unreinforced, at *S*=5 mm; (b) reinforced, *S*=5 mm; (c) reinforced, *S*=15 mm; (d) reinforced, *S*=20 mm

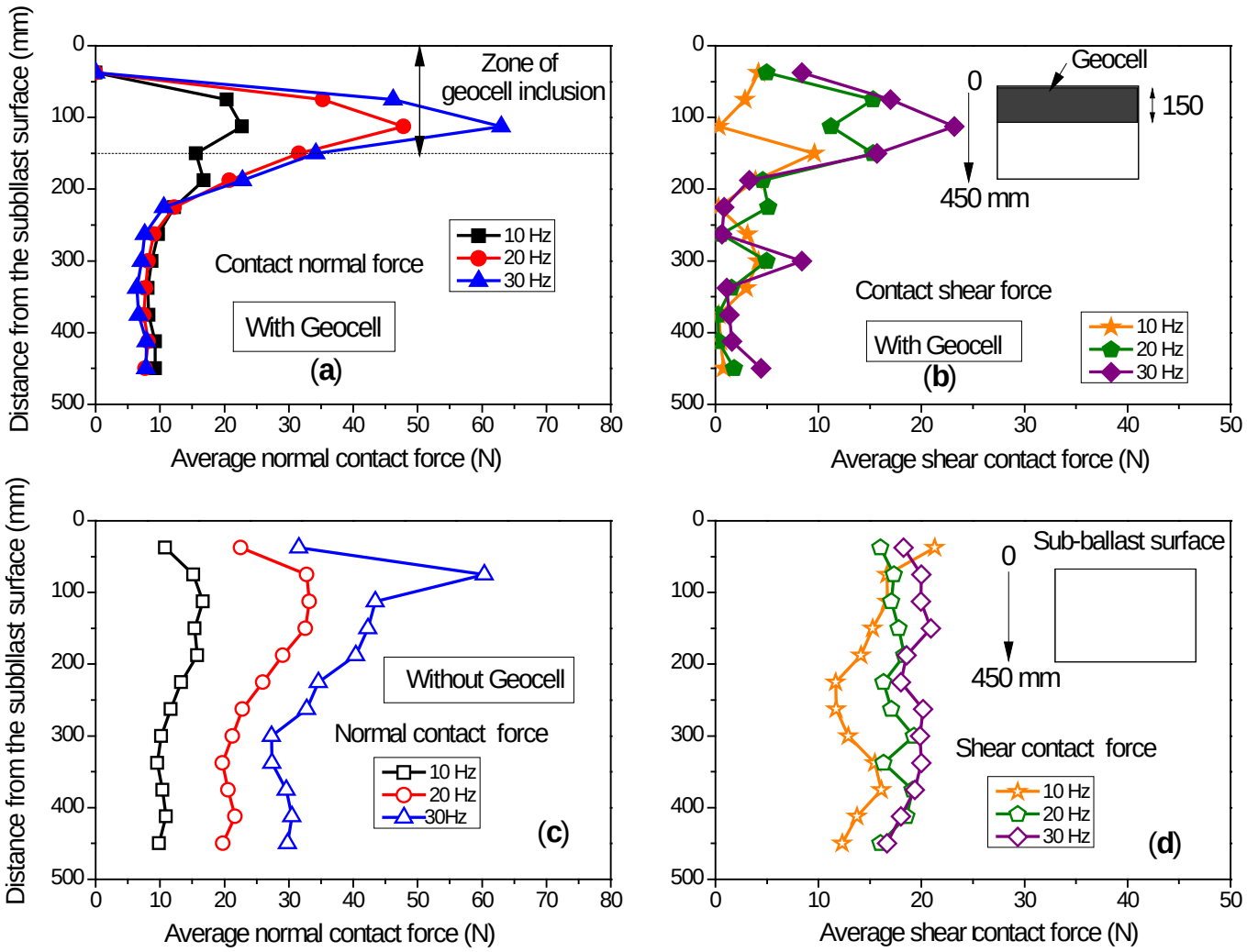

Figure 17. Distributions of contact normal and shear forces with varying depths in sub-ballast assemblies: (a) and (b) - with geocell inclusion; (c) and (d) - without geocell.